

## PRESSURE LOSS THROUGH THE BOTTOM END PIECE OF A NUCLEAR FUEL ASSEMBLY

Moysés A. NAVARRO<sup>1</sup> and André A. C. SANTOS<sup>2</sup>

<sup>1</sup> Brazilian Nuclear Energy Commission (CNEN/CDTN), Belo Horizonte, 30123-979, Brazil

<sup>2</sup> Federal University of Minas Gerais, (UFMG/DEMEC), Belo Horizonte, 31270-901, Brazil

### ABSTRACT

A study was conducted on the fluid dynamic characteristics of the bottom end piece of a nuclear fuel assembly. A commercial CFD code was used to simulate water flows through perforated plates in a square duct to evaluate both turbulence models and mesh refinement. Perforated plates with different diameter holes and one similar to the plate of the bottom end piece were simulated. The numerical results with the optimized mesh and SST  $k-\omega$  turbulence model showed a good agreement when compared with a conventional methodology (Idelchik). With the same mesh criteria and the SST  $k-\omega$  turbulence model were accomplished simulations in a standard bottom end piece, with some geometric simplifications. Experiments were also carried out to determine the pressure drop through the bottom end piece. The agreement between the numerical simulations and experimental results can be considered satisfactory but suggests further numerical investigations with bottom piece under real conditions of the experiment, without the geometric simplifications and with a gap between the piece and the wall of the flow channel. Additionally, other turbulence models should be appraised for this complex geometry.

### NOMENCLATURE

$DP$	differential pressure
$K$	pressure loss coefficient
$k$	turbulent kinetic energy
$L$	edge length
$P$	pressure
$q_m$	mass flow rate
$r$	radius
$V$	velocity
$\alpha$	angle
$\varepsilon$	dissipation
$\mu$	dynamic viscosity
$\rho$	density
$\omega$	specific dissipation

### INTRODUCTION

The end piece of a nuclear fuel element is constituted of a perforated plate responsible for the most of the pressure loss through the piece. The extremities of the guide tubes of the fuel assembly are stuck by a nut on the perforated plate. Besides this structural function the bottom perforated plate is a flow conditioner at the entrance of the fuel element. Recently, bottom end pieces manufactured with plates with small holes have been developed for an additional purpose: filter debris.

Perforated plates have also been studied as flow conditioners for measuring stations (Schlüter and Merzkirch, 1996; Spearman et al, 1996), as distillation trays to increase the heat and mass transfer between fluids (Lockett, 1986), as flow controller emerging from diffuser (Sahin and Ward-Smith, 1987).

The agreement between the pressure loss coefficients of perforated plates obtained from some experiments (Gan and Riffat, 1997) and that defined by Idelchik (Idelchik, 1994) are not always acceptable.

More recently, due to the great progress in the computational capacity, numeric modeling of flow through complex geometries such as perforated plates has been accomplished. As a consequence of this progress the commercial CFD codes have been strongly improved.

Although a considerable amount of studies on numerical simulation of flow through perforated plates (Erdal and Andersson, 1997; Erdal, 1997; Frattolillo and Massarotti, 2002) some issues related to turbulence models, near wall treatment and refinement of the mesh have still not been properly explained.

This work presents results of a numerical modeling of flow through different perforated plates in a square duct performed with the commercial code CFX 5.7.1. After turbulence models and mesh refinement studies, a suitable modeling was accomplished with a perforated plate similar to the bottom end piece of a nuclear fuel element. Finally, the whole end piece was simulated and this numerical result was compared with an experimental result.

### EXPERIMENTS

Figure 1 shows the schematic diagram of the experimental apparatus used in the measurement of the pressure loss through the bottom end piece of a nuclear fuel element. The bottom end piece is shown in Figure 2. The water flow was established in a about 1.4 m long, 0.23 x 0.23 m square duct. The uncertainty in the width of the duct was not evaluated but from the construction project it can reach up to +0.75 mm. The following conditions were established in the experiment:

Flow rate (orifice plate):  $49.7 \pm 0.5$  kg/s  
Pressure (gauge transmitter):  $1.04 \pm 0.01$  bar  
Temperature (thermocouple):  $40.9 \pm 1.1$  °C

The measurements of pressure drops at the positions shown in Figure 1 along the test section were performed by differential transmitters.

The pressure drops ( $DP$ ) and estimated uncertainties ( $\delta DP$ ) obtained in the experiments are shown in Table 1.

Taps 2-j	DP [mbar]	$\delta DP$ [mbar]
2-4	5.6	0.11
2-5	19.2	0.14
2-6	14.3	0.10
2-7	14.0	0.10

**Table 1:** Experimental results

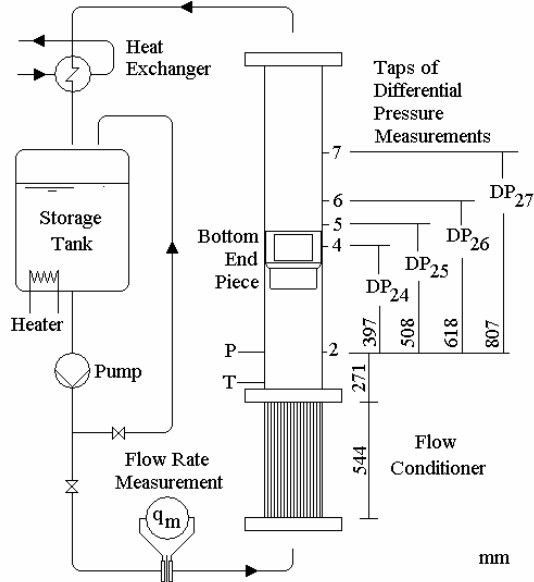


**Figure 1:** Experimental apparatus

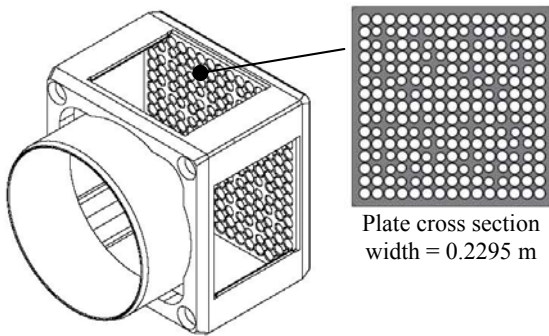


**Figure 2:** Bottom end piece

### THE NUMERIC MODELING

This numerical approach was performed using the commercial CFX 5.7.1 (2004) code. Water flows through perforated plates in a square duct were simulated under the same boundary conditions defined in the experiments with the bottom end piece. Different turbulence models based on the Reynolds Averaged Navier-Stokes (RANS) equations were used in the simulations. Different mesh refinements were also evaluated.

The pressure loss coefficients of the perforated plates, defined by eq. (1), obtained in the numeric simulations were also compared with values determined according to section 8 of the Handbook of Hydraulic Resistance by Idelchik (1994).

$$K = \frac{DP_s}{(1/2)\rho V^2} \quad (1)$$

where:

$DP_s$  = static pressure loss across the plate

$V$  = mean duct velocity

The  $DP$  assumed on  $K$  determination for the perforated plates is the difference between the average static pressure at the same upstream (tap 2) and downstream (tap 7) positions used in the experiments with the bottom end piece.

### Model Definition

Table 2 shows the geometric details of the distribution of the orifices, arranged in square array, on the perforated plates used in the numerical simulations.

	Number of orifices	d [mm]	pitch [mm]
Plates	81 (9x9)	18.88	25.50
	121 (11x11)	15.45	20.86
	225 (15 x 15)	11.33	15.30
BEP <sup>1</sup>	80	10.00	14.30
	145	12.00	

1 – Plate of the Bottom End Piece

**Table 2:** Details of the perforated plates

The same plate thickness of 20 mm and perforation ratio of 0.43065, of the plate of the bottom end piece were used in all the plates. The flow channel is a 0.2295 x 0.2295 m square duct with 0.7 m upstream and downstream lengths. In the simulation, the flow direction is in the z axis and the zero position is in the lower face of the plates.

To reduce the mesh size a symmetry slice of 1/8 was applied to the geometries as shown in Figure 3.

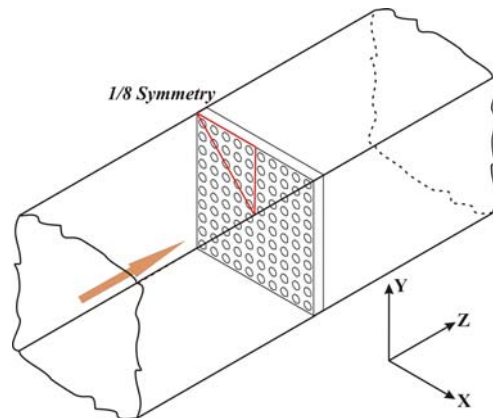


**Figure 3:** Flow duct with a perforated plate

Aiming to evaluate the influence of the chamfers on both ends of the holes a simulation with the 225 orifice plate and a chamfer of 1 mm/45°, similar to the plate of the bottom end piece was performed.

Figure 4 shows the geometric simplifications assumed for the bottom end piece. The simplifications were basically the removal of the bevel in the external corners. The reduction of the flow duct width from 0.23 m to the same width of the bottom end piece 0.2295 m was another simplification adopted. Both simplifications had the

objective to reduce the mesh dimension. The four positioning orifices were also eliminated in the numerical simulations.

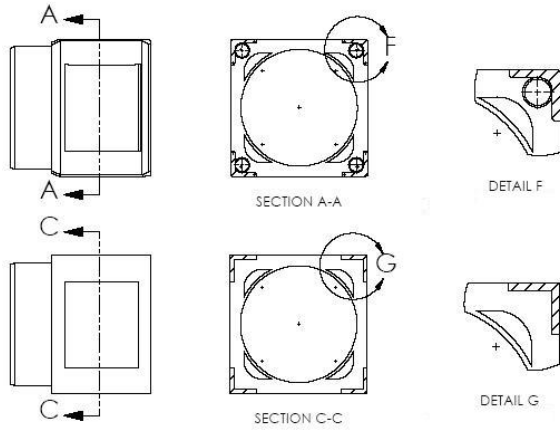


**Figure 4:** Simplifications in the bottom end piece geometry

### Boundary Conditions

The same pressure gauge 1.04 bar and water temperature 40.9 °C obtained in the BEP experiments were adopted in the simulations with the perforated plates. The inlet and outlet flow rates were reduced from 49.7 kg/s to 49.5 kg/s proportionally to the flow area reduction from the experimental flow duct (0.23 x 0.23 m) to the numerical simulation model (0.2295 x 0.2295 m).

The surfaces of the duct and plate were considered smooth and the inlet turbulence intensity was assumed to be 5% (although simulations made showed no significant influence in the pressure drop when values of 1 and 10% of turbulent intensity were applied). No thermal model was used since the experiments were considered adiabatic and isothermal.

### Turbulence Modeling

Three turbulence models of two equations which fall into the category defined as eddy viscosity models were used: the  $k-\epsilon$  model, developed by Launder and Spalding (1974) the  $k-\omega$  model, conceived originally by Kolmogorov (1942) and reformulated by Wilcox (2000); and the Shear Stress Transport (SST)  $k-\omega$  model, formulated by Menter (1994).

The  $k-\epsilon$  turbulence model assumes that the turbulence viscosity is related to the turbulence kinetic energy and dissipation. In CFX the  $k-\epsilon$  model uses a scalable wall-function approach to improve the near wall treatment which is made with the log-wall function. The basic idea behind the scalable wall function is to limit a lower value for the dimensionless distance from the wall used in the log-law in such a way that all the mesh points are outside the viscous sub layer. In this way all fine mesh inconsistencies near the wall can be avoided.

The  $k-\omega$  turbulence model assumes that the turbulence viscosity is linked to the turbulence kinetic energy and the specific dissipation rate. In CFX the automatic wall treatment is used. This treatment automatically switches from the wall-functions to low-Reynolds near wall formulation as the mesh is refined.

In the Shear Stress Transport (SST)  $k-\omega$  model the turbulent viscosity is modified to account for the transport of the turbulent shear stress. The model uses a function to blend the accurate near the surface  $k-\omega$  model and the  $k-\epsilon$

formulation in the outer region. This model uses the same automatic near wall treatment used in the  $k-\omega$  model.

### Mesh Definition

In the CFX-Mesh the algorithms *Delaunay Mesher* and *Advancing Front Mesher* were used to generate the surface and the volumetric mesh, respectively. The global mesh scaling adopted in all simulations was of 16.5 mm. Mesh controls were used to refine the superficial and volumetric mesh in specific regions. The perforated plate region was refined to capture better the rapid flow contraction and expansion. A refinement plane (*Triangle Control*), with a radius of influence of 10 mm was defined in the middle height of the plate and the angular division of the orifice was used as a parameter to determine the mesh edge length on this plane. The eq. (2) shows the adopted relationship between the edge length ( $L$ ), the angular division ( $\alpha$ ) and the radius ( $r$ ) of the orifice plate. This criterion allows a better definition of the circular form of the orifices. Several simulations were performed on the perforated plate with 81 orifices applying different angular divisions according to Table 2. A smooth expansion factor of 1.1 was applied to enhance accuracy.

$$L = r\sqrt{2 - 2\cos\alpha} \quad (2)$$

The downstream region of the perforated plate was also refined to capture the pressure recuperation that occurs in this region. Another refinement plane (*Triangle Control*) was used and its position for each of the plates was defined after extensive simulations. It was also found that the abrupt recovery of the pressure occurs at about six orifice diameters downstream of the plate. An expansion factor of 1.2 was assumed on this refinement plane. The  $L/2r$  ratio was kept about 0.15 for all simulations on this plane.

Near the walls a structured mesh (*inflation*) was used to capture the effects of the boundary layer. An effort was made to maintain the value of the first dimensionless wall parameter less than 2, as is recommended in CFX for models based on the  $k-\omega$  wall treatment. Twenty layers were used with an expansion factor of 1.2.

On the bottom end piece a third refinement plane was used to refine the bottom support region. On this plane a edge length of 4 mm with an expansion factor of 1.2 was applied.

Details of the inflation near the wall and of the localized refinements on an axial central plane of the 81 orifice plate are shown in Figure 5.

Table 3 shows the results obtained with different mesh refinements and turbulence models used in the numerical simulation with the 81 orifices plate. The pressure drop coefficients are compared with the obtained from the Idelchik handbook,  $K_I = 4.18$ .

Figure 6 shows more clearly that the  $K$  values obtained with the  $k-\omega$  and  $k-\epsilon$  turbulence models are smaller than those obtained with the SST model which reproduces relatively well the  $K$ -Idelchik value for the better refinements. Small differences between the coefficients can be observed for edge lengths smaller than 1.5 mm.

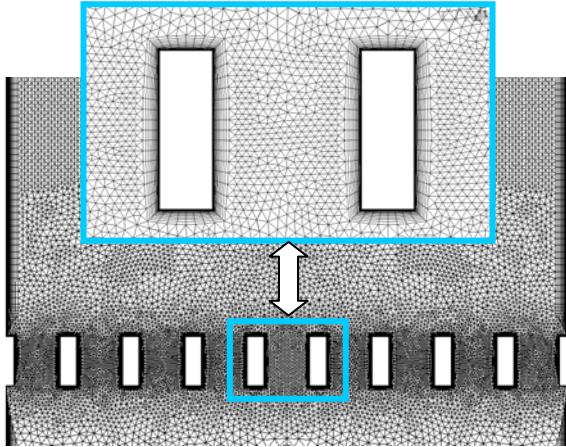


**Figure 5:** Details of the mesh in the region of the plate with 81 orifices

Refinement – $\alpha/L$ [degree/mm]	Turbulence Model	$K$	$(K-K_I)/K_I$ [%]
12/1.974	$k-\varepsilon$	3.79	-9.3
	$k-\omega$	3.81	-8.9
	SST	3.88	-7.2
9/1.481	$k-\varepsilon$	3.9	-6.7
	$k-\omega$	3.97	-5.0
	SST	4.13	-1.2
6/0.988	$k-\varepsilon$	3.9	-6.7
	$k-\omega$	3.97	-5.0
	SST	4.20	0.5
4/0.659	$k-\varepsilon$	3.91	-6.5
	$k-\omega$	3.95	-5.5
	SST	4.17	-0.2

**Table 3:** Pressure loss coefficients for the different mesh refinements and turbulence models

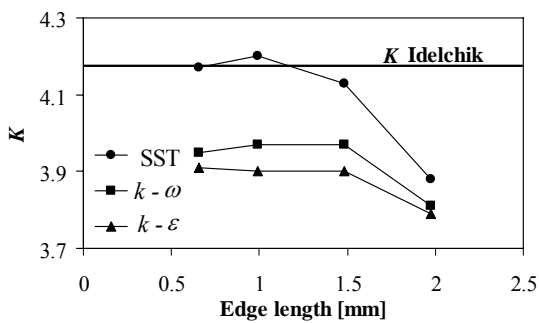


**Figure 6:** Influence of the mesh refinement and turbulence models on the pressure drop coefficient

Figure 7 shows the static pressure behavior along a central line of the duct for different mesh refinements applied also on the 81 orifice plate. It can be seen that the pressure loss inside the holes increases as the mesh refinement increases. Details of velocity profile at entrance of a hole are shown in Figure 8 for the four refinements studied. It can be observed that the mesh with smaller edges captures better the flow detachment at the entrance of the hole and the flow downstream recirculation near the wall of the hole. Similarly, Figures 9 and 10 show that the SST turbulence model captures better the same flow situation at the hole entrance.

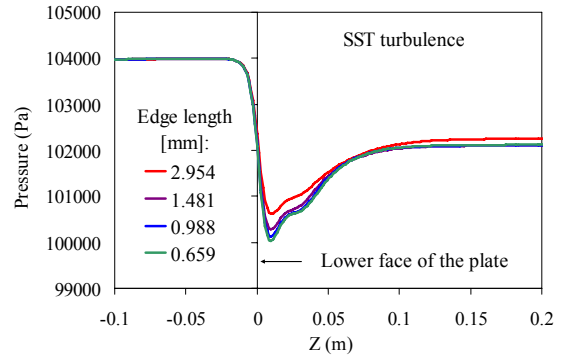


**Figure 7:** Influence of the mesh refinement on the pressure drop

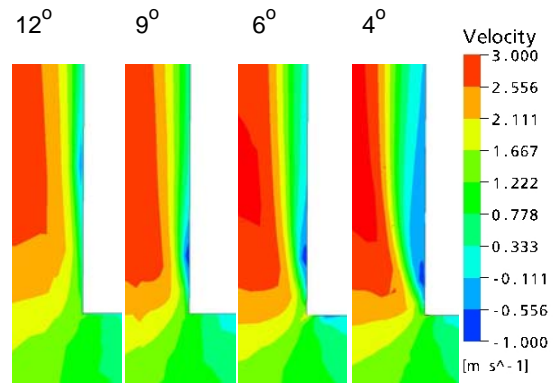


**Figure 8:** Details of the velocity profile at the entrance of a hole for different edge lengths ( $\alpha$ ) for the plate with 81 holes

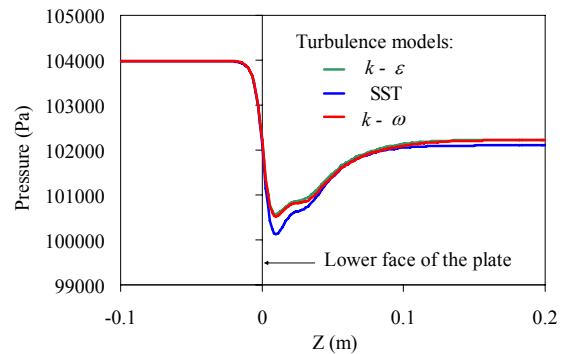


**Figure 9:** Influence of the turbulence models on the pressure

The results of the simulations performed with the 81-hole plate led to the definition of the mesh parameters and turbulence model adopted for the simulations with the other perforated plates. The mesh criterion remained the same and in the plate region the mesh edge length obtained with  $\alpha = 6^\circ$  in eq. (2) was assumed for all the other perforated plates. This was adopted to minimize the computational effort maintaining an acceptable mesh quality. This can be seen in Table 4 where the numbers of volumetric elements of all obtained meshes are shown.

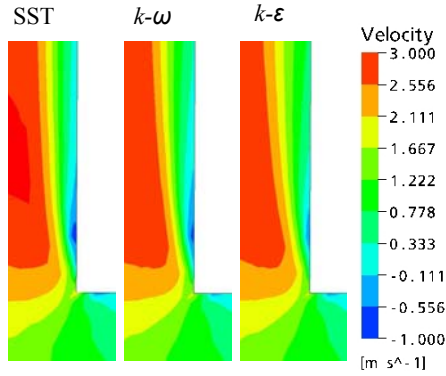


**Figure 10:** Details of the velocity profile at the entrance of a hole for different turbulence models for the with 81-hole plate

For the mesh with 4° of refinement, the number of elements is more than double of the mesh with 6°. For more complex geometries, such as the BEP, the generated mesh with 4° of refinement would have an excessive size, making it impossible to simulate with the available hardware available. All simulations were performed though parallel runs on two Pentium 4 HT PCs with 4 GB of RAM memory. The simulations took 1.5 (81 holes – 12°) to 7.5 (225 holes with chamfer) hours for the perforated plates and 15 hours for the BEP. The turbulence model SST was used in the simulations of the flow with the other perforated plates.

Plate/BEP	$\alpha$ -[degree]	Number of elements
81	12	1154450
	9	1561866
	6	2306802
	4	4664806
121	6	3589958
225	6	6047291
225 <sup>1</sup>	6	6285987
BEP	6	6849840

1 - Orifices with chamfer

**Table 4:** Number of volumetric elements

## RESULTS

Table 5 compares the pressure drop coefficients obtained in the numeric simulations with the Idelchik coefficients, for the other perforated plates. In spite of the same perforation ratio for all of the plates, a reduction of the pressure loss coefficient with the decrease of the orifice diameter was verified. Figure 11 shows the profiles of the static pressure along the central line of the flow duct with different perforated plates. A reduction of the recovery pressure distance downstream the perforated plate with the decreasing of the orifice diameter was observed.

A simulation was performed, with the same mesh parameters and SST turbulence model, on a plate with 225 orifices with beveled edges on both ends, like the plate of the bottom end piece. As expected, the chamfer at the entrance of the orifice produces a smooth area reduction that leads to a lower pressure drop through the plate. The coefficient obtained with the beveled edge chamfers is

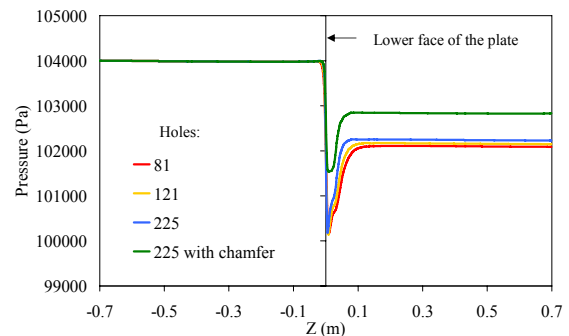
about 37 % lower than the coefficient for the sharp edged plate.

Plate	K-CFX	K-Idelchik	Difference %
81	4.20	4.18	0.48
121	4.07	4.00	1.75
225	3.96	3.86	2.59
225 <sup>1</sup>	2.49	-	-37.12 <sup>2</sup>

1 - Orifices with chamfer

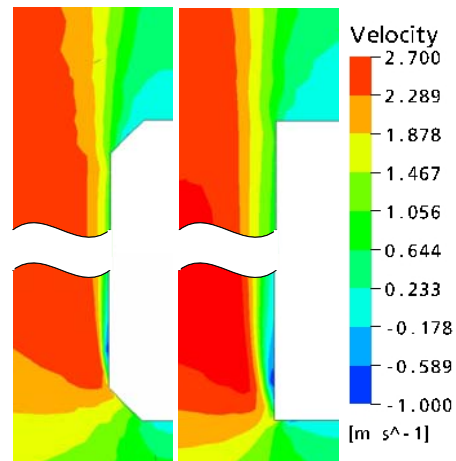
2 - Relative to the numerical result without chamfer

**Table 5:** Pressure loss coefficients for perforated plates



**Figure 11:** Static pressure along the duct with different perforated plates

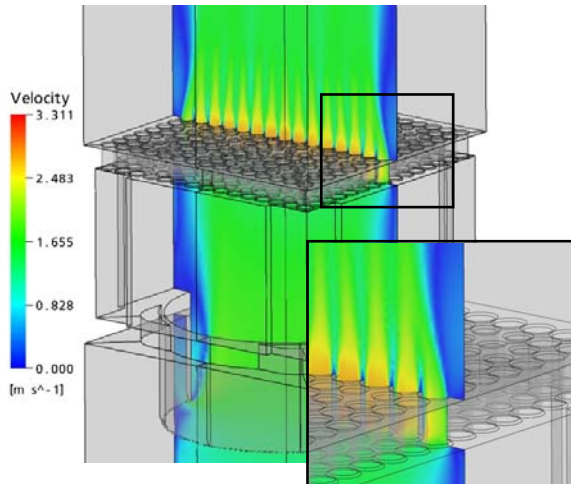
Figure 12 compares the velocity color profiles of a hole with and without chamfer. It can be observed that a smaller separation occurs at the entrance of hole and that the boundary layer is thinner when the chamfer is present. At the exit of the hole the gradual increase of the diameter causes a smoother velocity profile.



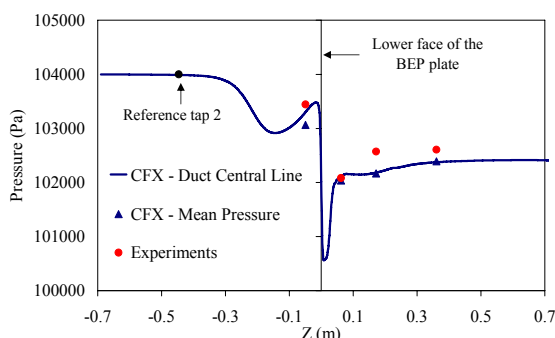
**Figure 12:** Differences between the velocity profiles at an orifice with and without chamfer

Figure 13 shows the velocity distribution found on the central plane of the bottom end piece and Figure 14 compares the experimental and numerical results of pressure loss along the duct with the bottom end piece. In Figure 14 shows a difference of 15.5% between the experimental and numerical  $K_{BEP}$  results. A great part of this difference can be attributed to the removal of the gap between the piece and the wall of the duct (minimal 0.25

mm – maximal 0.625 mm) in the numerical simulation. Some attempts were made to generate a mesh with a 0.4 mm gap, without the simplifications assumed in the geometry of the bottom end piece, but due to computational limitations it was not possible. A mesh to properly simulate the gap would have approximately 18000000 elements.



**Figure 13:** Velocity distribution in a central plane of the bottom end piece



**Figure 14:** Static pressure along the duct with the bottom end piece: experiments x numerical simulation

## CONCLUSION

In this analysis, experimental data concerning a pressure drop through a bottom end piece of a nuclear fuel element have been experimentally determined and compared to results from numerical simulations conducted with a commercial CFD code (CFX 5.7.1).

Previously, a numerical study was performed on 3 perforated plates with different number of holes to determine optimum mesh and turbulence models. Three turbulence models of two equations were used: the  $k-\epsilon$  model, the  $k-\omega$  model and the Shear Stress Transport (SST)  $k-\omega$  model. Mesh controls were used to refine the superficial and volumetric mesh in specific regions of the perforated plates to capture better the rapid flow contraction and expansion. The pressure drop coefficients obtained in these simulations with the SST turbulence model were compared with those from Idelchik methodology and showed a good agreement. It was also verified that the chamfers on the ends of the holes generated a lower pressure drop through the plates.

The same mesh criterion and the SST turbulence model were adopted in the bottom end piece simulations. Same simplifications were assumed in the geometric form of the piece which were responsible for the discrepancies obtained in the results. Limitations on the computational capacity disabled an appropriated simulation of the gap between the bottom end piece and the flow duct wall which can reach up to 0.625 mm. Further investigations are still necessary to evaluate the flow behavior with the gap.

Other turbulence models need to be appraised in simulations of complex geometries such as the bottom end piece.

Despite the dependence of the numerical results on the mesh refinement and the turbulence model, the study indicated that the CFD codes can play an important role in the development of pieces with complex geometries, optimizing experiments and aiding in the analysis of the experimental results.

## REFERENCES

- CFX-5.7.1, (2004), "User manual", ANSYS-CFX.
- ERDAL, A. and ANDERSSON, H. J., (1997), "Numerical aspects of flow computation through orifices", *Flow. Meas. Instrum.*, 5, 27-37.
- ERDAL, A., (1997), "A numerical investigation of different parameters that affect the performance of a flow conditioner", *Flow. Meas. Instrum.*, 8, 93-102.
- FRATOLILLO, A. and MASSAROTTI, N., (2002), "Flow conditioners efficiency a comparison based on numerical approach", *Flow Meas. Instrum.*, 13, 1-11.
- GAN, G. and RIFFAT, S. B., (1997), "Pressure loss characteristics of orifice and perforated plates", *Experimental Thermal and Fluid Science*, 14, 160-165.
- IDELCHIK, I. E., (1994), "Handbook of hydraulic resistance", third edition, CRC Press Inc., Boca Raton.
- KOLMOGOROV, A. N., (1942), "Equation of motion of an incompressible turbulent fluid", *Izv. Akad. Nauk SSSR Ser. Phys.* VI, 56.
- LAUNDER, B. E. and SPLADING, D. B., (1974), "The numerical computation of turbulent flow", *Computer Methods in Applied Mechanics and Energy*, 3, 269-289.
- LOCKETT, M. J., (1986), "Distillation tray fundamentals", Press, Cambridge, UK.
- MENTER, F. R., (1994), "Two-equation eddy-viscosity turbulence models for engineering applications", *AIAA-Journal*, 32, 269-289.
- SAHIN, B. and WARD-SMITH, A. J., (1987), "The use of perforated plates to control the flow emerging from a wide-angle diffuser, with application to electrostatic precipitator design", *J. Heat Fluid Flow*, 8, 124-131.
- SCHLÜTER, Th. and MERZKIRCH, W., (1996), "PIV measurements of the time-averaged flow velocity downstream of flow conditioners in a pipeline", *Flow Meas. Instrum.*, 7, 173-179.
- SPEARMAN, E. P., SATTARY J. A. and READER-HARRIS, M. J., (1996), "Comparison of velocity and turbulence profiles downstream of perforated plate flow conditioners", *Flow Meas. Instrum.*, 7, 181-199.
- WILCOX, D. C., (2000), "Turbulence modelling for CFD", DCW Industries, La Canada.